Cooperative action of KIF1A Brownian motors with finite dwell time

David Oriola* and Jaume Casademunt
Departament d'Estructura i Constituents de la Matèria, Facultat de Física, Universitat de Barcelona, Avinguda Diagonal 647, E-08028 Barcelona, Spain

(Received 1 December 2013; revised manuscript received 13 February 2014; published 31 March 2014)

We study in detail the cooperative action of small groups of KIF1A motors in its monomeric (single-headed) form within an arrangement relevant to vesicle traffic or membrane tube extraction. It has been recently shown that under these circumstances, the presence of a finite dwell time in the motor cycle contributes to remarkably enhance collective force generation [D. Oriola and J. Casademunt, Phys. Rev. Lett. **111**, 048103 (2013)]. We analyze this mechanism in detail by means of a two-state noise-driven ratchet model with hard-core repulsive interactions. We obtain staircase-shaped velocity-force curves and show that motors self-organize in clusters with a nontrivial force distribution that conveys a large part of the load to the central motors. Under heavy loads, large clusters adopt a synchronic mode of totally asymmetric steps. We also find a dramatic increase of the collective efficiency with the number of motors. Finally, we complete the study by addressing different interactions that impose spatial constraints such as rigid coupling and raft-induced confinement. Our results reinforce the hypothesis that the specificity of KIF1A to axonal vesicular transport may be deeply related to its high cooperativity.

DOI: 10.1103/PhysRevE.89.032722 PACS number(s): 87.17.Aa, 87.16.Wd, 87.16.Nn, 05.40.−a

I. INTRODUCTION

Intracellular traffic in cells is mainly enabled by kinesins and dyneins, which transport a large variety of cargoes along microtubule (MT) filaments [1–4]. Some of the most demanding conditions for such tasks are found in neurons [5–7]. Proteins required in synaptic terminals are synthesized in the soma of the cell and must be transported through axons. In addition to the long distances that vesicles need to travel (ranging from millimeters up to even meters), the densely crowded axoplasm and the possibility of traffic jams may put at risk the delivery of cargoes at their destination, with severe consequences for neuronal function. For instance, impaired axonal transport due to the formation of traffic jams has been associated with neurodegenerative diseases [8,9]. Long-range processivity of vesicles, that is, the capacity to travel long distances without detachment from the microtubules, is ensured by combining large numbers of motors available on the vesicle. However, the capacity to exert forces on a vesicle by a collection of motors is limited by the liquidlike nature of the vesicle membrane. This implies, for instance, that the accumulation of large numbers of conventional kinesin motors would not furnish the capability to eventually overcome obstacles or traffic jams that impede the advance of a vesicle [10–12]. Understanding the mechanisms of motor self-organization designed to secure robust transport, in particular with respect to the generation of large forces, is thus of primary importance.

Recently, there has been increasing interest in a member of the kinesin-3 family, the kinesin KIF1A [5,13–17], which is specific for the transport of synaptic vesicle precursors in axons. This motor has been reported to work processively *in vitro* in a monomeric (single-headed) form by means of a two-state noise-driven ratchet mechanism, being a natural prototype of a Brownian motor [13,15,18–20]. The motor combines a strongly bound state to the MT with a weakly bound state in which the K loop of the motor domain interacts with the MT and prevents full detachment from the filament [14]. In this state, the motor is able to diffuse freely along the filament. Single-molecule experiments using monomeric KIF1A have reported velocities of 0.2 μm/s and stall forces around $\simeq$0.1 pN [15], which reflect the inefficiency of the noise-driven ratchet mechanism for a single motor compared to the hand-over-hand mechanism typical of conventional dimeric (double-headed) kinesin (kinesin-1 family, also referred to as KIF5), with stall forces around 60 times larger. KIF1A has been found to operate *in vivo* in its dimeric form [21]; however, the motor preserves a weakly bound diffusive state similar to that of its monomeric form, which is expected to weaken the motor and reduce its efficiency, similarly to its single-headed counterpart and clearly at odds with the particularly demanding conditions of axonal transport. We previously showed that the presence of a weakly bound state is suitable for the cooperative action of Brownian motors under unequal loading in configurations relevant to the transport of soft cargoes [22,23]. In such conditions, it was proposed that KIF1A could achieve collective forces proportional to the number of motors at finite velocity. Recently, we reported that the existence of a finite dwell time in the motor cycle could strongly enhance the collective force generation of groups of motors, thus further increasing their cooperativity [24]. The present paper extends the results presented in Ref. [24] by studying in detail different observables for KIF1A motor clusters such as velocity-force (VF) relationships, cluster force distributions, and efficiencies; considering different types of interactions between motors that are relevant to different situations both *in vitro* and *in vivo*.

II. MODEL FOR KIF1A DYNAMICS

We consider the general problem of N KIF1A motors moving along a one-dimensional track with periodicity l. The dynamics of the system are defined by a set of N Langevin

*oriola@ecm.ub.edu

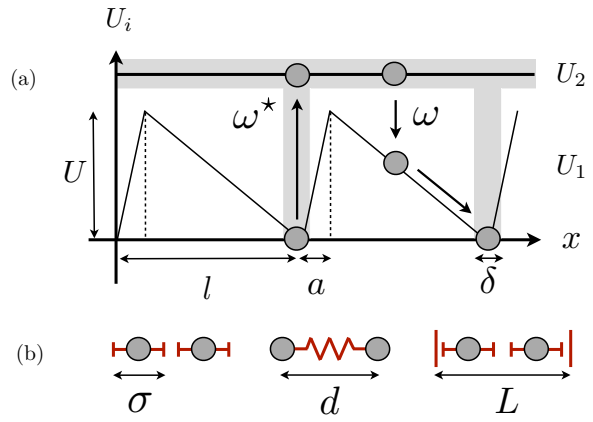

FIG. 1. (Color online) Description of the model. (a) Two-state ratchet model for monomeric KIF1A. Motors switch stochastically between the states $k = 1,2$ with potentials U_1 and U_2, respectively. Excitations are localized in regions of size δ around the minima of U_1, whereas decays are delocalized. The average excitation and decay rates read $\omega^\star$ and ω, respectively. Gray zones depict where transitions are allowed. (b) Main motor-motor interactions: hard-core repulsion (left), rigid coupling (center), and raft-induced interactions (right) (see Secs. III and IV). Small circles indicate the motor position and the red drawings indicate the type of interaction.

equations for the set of positions $\boldsymbol{x}(t) = \{x_1(t), \ldots, x_N(t)\}$:

$$\lambda \dot{x}_i = -U'(x_i, k_i) - \sum_{k \neq i} W'(x_i - x_k) - F\delta_{1i} + \zeta_i(t), \quad (1)$$

where $i = 1, \ldots, N$, λ is the friction coefficient, and $\zeta_i(t)$ is a Gaussian white noise for the ith motor that follows the relation $\langle \zeta_i(t)\zeta_j(t')\rangle = 2k_BT\lambda\delta_{ij}\delta(t - t')$. The set $\boldsymbol{k}(t) = \{k_1(t), \ldots, k_N(t)\}$ defines the configuration of the system at time t, where $k_i(t) = \{1,2\}$ is a discrete stochastic variable that describes the state of the ith motor. The two possible states correspond to two different conformations of the motor domain, with their respective potential landscapes $U(x_i, k_i)$. When KIF1A captures an adenosine triphosphate (ATP) molecule, the motor switches to a weakly bound state ($k_i = 2$). In this state, KIF1A diffuses along the filament with diffusion coefficient D subject to a constant potential $U_2 \equiv U(x_i, 2)$. In contrast, in the absence of ATP, the motor is strongly bound to the filament ($k_i = 1$) and subject to a periodic ratchet potential $U_1 \equiv U(x_i, 1)$ similar to the one depicted in Fig. 1(a). Each motor switches its state independently and follows its particular kinetics. Since KIF1A carries soft cargoes, motors are not fixed in the cargo reference frame and they interact via a given potential $W(\xi)$. Finally, F is the tangential load originated by the cargo. This force is applied only to the foremost motor that conveys the load to the rest. This nonequal loading has already been shown as the main reason for the appearance of cooperativity in the system [22,23]. Next we need to describe the state dynamics. We define the average excitation rate $\omega^\star$, which depends essentially on the time required to capture an ATP molecule. We assume that the molecule is allowed to get excited only in a small neighborhood of size δ around the potential minima, that is, $\delta \ll l$. This condition follows from the fact that the motor is not likely to capture an ATP molecule during the power stroke (i.e., sliding down the sawtooth potential). On the other hand, we assume that thermal decays are delocalized, with an average decay rate ω [Fig. 1(a)]. Motors get excited and decay stochastically, with exponential distributed times having average values $1/\omega^\star$ and $1/\omega$, respectively.

The presence of an external load F applied to the foremost motor drives the spontaneous formation of a fluctuating cluster. When the steady state is reached, the velocity of an N-motor cluster coincides with that of the first motor $V_N(F) = \langle \dot{x}_1 \rangle$. On the other hand, the collective stall force is usually defined as the necessary force to stall the cluster. However, it is quite common that for large numbers of motors the collective VF curves fall to very small values at forces significantly smaller than the stall force, implying the existence of an apparent stall force that scales differently with N respect to the actual stall force [10,24]. In such cases it is useful and convenient to define an apparent stall force F_s by a condition of the type $V_N(F_s) = V_c$, where V_c is a small cutoff velocity. Hereinafter we will use the term stall force and the notation $F_s(N)$ to denote the apparent stall force of an N-motor cluster, unless otherwise indicated. Finally, the collective efficiency $\eta_N(F)$ in the biological context is usually defined as [25]

$$\eta_N(F) = \frac{F V_N(F)}{r_N(F)\Delta\mu}, \quad (2)$$

where $r_N(F)$ is the collective chemical reaction rate dependent on the applied force. In our case the calculation of this rate equals the number of excitations per unit time for all the motors and $\Delta\mu$ corresponds to the chemical potential difference for ATP hydrolysis. Since we will work in far-from-equilibrium conditions (i.e., $\Delta\mu \gg k_BT$) we neglect thermal activations.

Next we discuss the proper parameters to model a single-headed KIF1A motor *in vitro*. Table I shows the main selected parameters in our study.

The most salient feature of single-headed KIF1A is that the ability to advance along the MT relies on thermal diffusion in the weakly bound state. *In vitro* experiments have reported diffusion coefficients in the range of 20–40 nm^2/ms, which involve motor excursions much larger than the ratchet periodicity of 8 nm [13,15]. We will consider 20 nm^2/ms as a reasonable value. The characteristic rates ω and $\omega^\star$ are found in the literature within the range of hundreds of Hz. Whereas ω is a parameter coming from the affinity between the motor domain and the MT, $\omega^\star$ depends on ATP concentration in the solvent. Experimental data suggest that $\omega^\star \leqslant 250\ \text{s}^{-1}$ and $\omega \simeq 250\ \text{s}^{-1}$ [13,15,16]. The asymmetry a

TABLE I. Realistic values of the main parameters for the modeling of monomeric KIF1A motors *in vitro*. The values are extracted mainly from [13,15,16].

Parameter	Value
MT periodicity	$l = 8$ nm
ratchet asymmetry	$a = 1.6$ nm
diffusion coefficient	$D = 20\ \text{nm}^2/\text{ms}$
excitation rate	$\omega^\star \leqslant 250\ \text{s}^{-1}$
decay rate	$\omega = 250\ \text{s}^{-1}$
ratchet potential maximum	$U = 20k_BT$

of the ratchet is an adjustable parameter for the model that is difficult to grasp from experiments. The asymmetry reduces the overall velocity of the system and can lead to nontrivial effects especially in the limit of weak noise [23]. For our purposes, we adjust this parameter to 20% of the periodicity length. Finally, the motor size σ is carefully chosen to avoid possible commensurability effects [22,23]. In Sec. IV C we will study in detail the implications of this parameter in the study of the collective stall force of the system.

III. HARD-CORE REPULSIVE INTERACTIONS

To study the dynamics of N interacting motors, we first consider hard-core repulsion between them. For practical reasons we use a truncated Lennard-Jones potential

$$W_{HC}(\xi) = 4\epsilon\left[\left(\frac{\sigma}{\xi}\right)^{12} - \left(\frac{\sigma}{\xi}\right)^{6}\right] \tag{3}$$

for $\xi < 2^{1/6}\sigma$ and zero otherwise, where ϵ is taken large enough to ensure that the interaction is effectively hard core for $\xi < \sigma$.

A. Dwell time effect for $N = 2$

Excitations of motors are localized in regions of size $\delta \ll l$ centered in the minima of the ratchet potential. Once a motor enters this region, it waits a certain amount of time given by an exponential dwell time distribution with average dwell time $1/\omega^\star$. We define $\beta \equiv \omega/\omega^\star$ so that the previous studies in Refs. [22,23] with negligible dwell time correspond to the case $\beta = 0$. In a first approximation, we will consider that once the motor enters the region δ it stays in the minimum of the ratchet without fluctuating and hence it cannot escape from the region by thermal fluctuations. This condition will loosen and be further discussed in Sec. III B. In Fig. 2(a) of Ref. [24], the effect of the dwell time on the stall force is shown. The KIF1A velocity at zero load is $V_1 = 0.15\,\mu$m/s for $\beta = 2.5$ and the stall force is $\simeq$0.1 pN. These results are very similar to those found experimentally [15]. On the addition of a second motor, we find a remarkable enhancement of the VF curve with a consequent increase on the stall force of the cluster. If the dwell time is set to zero ($\beta = 0$) [Fig. 2(a), inset, of Ref. [24]] the naive extensive scaling $F_s(N) = NF_s(1)$ is approximately correct, consistently with the validity of the mean-field description discussed in Ref. [23] for sufficiently large diffusion. However, for $\beta \neq 0$, we find that $F_s(2)$ may be up to three times larger than $F_s(1)$ [Fig. 2(b) of Ref. [24]]. The stall force of the cluster grows with β until saturation, while the velocity at zero load rapidly decreases. The reason for the enhancement of the stall force can be explained in simple terms by considering two interacting motors.

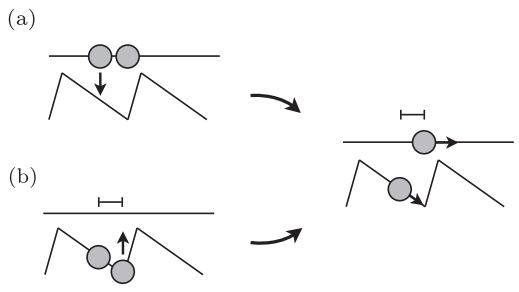

FIG. 2. Schematic description of the two cooperative mechanisms for the case of hard-core repulsion. (a) "Down-push" mechanism: Initially, the motor in the back decays and slides down the potential pushing the foremost motor to the next site. (b) "Up-push" mechanism: The leading motor is waiting for an ATP molecule while the second one is blocked in the ratchet slope. Once the leading motor is excited, the second motor pushes the foremost like in mechanism (a). The segment indicates that motors are found in contact.

Let us consider the configuration in Fig. 2(a), which was first discussed in [22]. Initially, the motor in the back decays and slides over the potential pushing the foremost motor to the next period of the MT. This mechanism is sensitive to the external force since both motors can drift backward when they are found in the initial configuration and holds only for $F \leqslant 2F_s(1)$. Therefore, it cannot be responsible for the stall force enhancement. Moreover, the strength of this mechanism is proportional to the ATP concentration in the solvent since the initial state requires the two motors to be found in state $k = 2$. Consequently, when β increases the mechanism loses strength, in contradiction to the curve in Fig. 2(b) of Ref. [24]. We call this mechanism a "down-push".

Now let us focus on the mechanism initiated from the configuration in Fig. 2(b). We notice that this configuration is only possible if $\beta \neq 0$ since the two motors are found together in state $k = 1$. The leading one is waiting for ATP, while the second one is blocked on the ratchet slope. Once the leading motor is excited, the second motor pushes the foremost in the same way as before. We call this mechanism an "up-push". However, in this case the initial configuration remains unaffected for small forces $F \sim k_B T l/l_D^2$, where $l_D \equiv \sqrt{2D/\omega}$ and the "up-push" mechanism is able to work for $F > 2F_s(1)$. Furthermore, this mechanism is ATP dependent and its strength saturates for very low concentrations, as shown in Fig. 2(b) of Ref. [24]. The same results can be studied more precisely using a lattice model [24].

B. Dwell time effect for arbitrary N

Next we study the VF relationship for an arbitrary number of motors. In Fig. 3(a) we find a dramatic enhancement of the force at finite non-negligible velocities as we increase N. Although the velocity at zero load is the same for different N, the stall force is largely increased. We also note a remarkable complex shape of the curves, which resemble a staircase. This effect is a consequence of the inhomogeneous motor density distribution in the cluster and the particular high noise intensity in the system. For relatively low forces, the external force is conveyed only to a reduced fraction of active motors in the center of the cluster (see Sec. III D), while those in the rear behave much more diffusively and remain loosely bound to the active group [Fig. 3(b)]. The successive plateaus correspond to the recruitment of new motors by the active group. Indeed, as the force is increased, the new motor interacts more often with the active group and thus becomes progressively more cooperative. This partially compensates for the decrease of velocity for a certain range of forces. This phenomenon becomes ineffective whenever the force reaches a multiple of $\sim U/l$, which is the typical ratchet force. At this point,

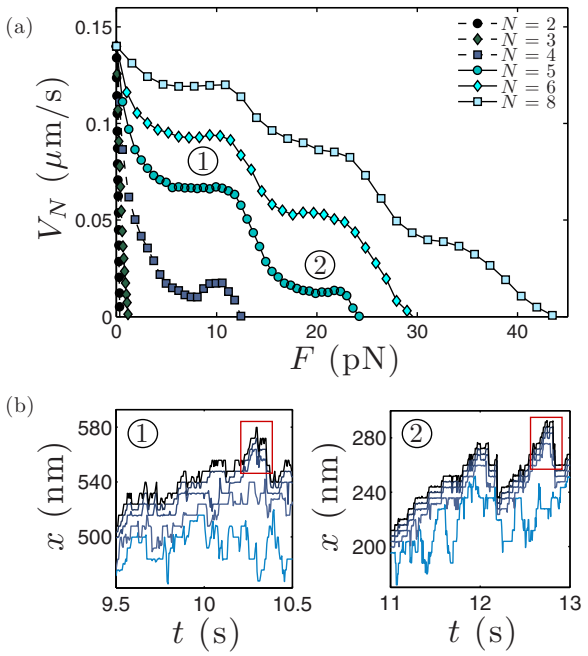

FIG. 3. (Color online) (a) Plot of VF curves for different N, with $\beta = 2.5$, $\sigma/l = 0.521$, and $\delta/l = 0.02$. The collective stall force grows rapidly with N in a nonlinear fashion. Moreover, the high diffusive environment induces a staircase shape of the VF curves. Data correspond to the case where motors cannot fluctuate in ratchet minima. (b) Typical motor trajectories for cases 1 ($F = 8$ pN) and 2 ($F = 20$ pN) in (a). Red squares show the active motors in the front, which are generally three in case 1 and four in case 2.

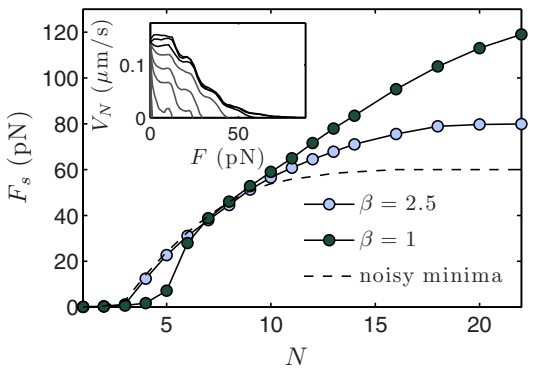

FIG. 4. (Color online) Plot of F_s vs N for $\beta = 1,2.5$ (circles) and for noise in the minima ($\beta = 2.5$ and $\delta/l = 0.02$, dashed line). We differentiate a steep enhancement for small clusters and a saturation regime for large clusters assuming a cutoff velocity $V_c \simeq 10^{-4}$ μm/s. The inset shows VF curves for $N = 2$–8 (gray) and $N = 10,15,20$ (black) for $\beta = 2.5$. We notice the long tails near stall force conditions.

both cooperative mechanisms in Fig. 2 fail and motors can be dragged back over the ratchet slope. Therefore, each plateau in Fig. 3(a) can be identified as the recruitment of a new motor by the active part of the cluster. For instance, for $N = 5$ the first plateau corresponds to typically three active motors and the second plateau to four active motors, as shown in Fig. 3(b). This mechanism also persists for backward movement until the recruitment of the totality of motors (see Sec. III C, Fig. 5, inset).

In Fig. 4 we study in detail the scaling of F_s with N for different possible values of β (circles) and also in the case of allowing fluctuations of the motors in the ratchet minima (dashed curve). We notice a steep enhancement for low N and saturation of the stall force for large N. The presence of noise in the minima changes effectively the average excitation rate to an effective average rate $\omega'^{\star}$. Once a motor drifts out of the region δ by thermal fluctuations, it soon falls back in the minimum again, thus waiting again for ATP. Consequently, the addition of noise in the ratchet minima corresponds to a smaller effective excitation rate $\omega'^{\star} < \omega^{\star}$ (or equivalently $\beta' > \beta$).

In Fig. 4 (inset) we observe the saturation of the VF curves and the occurrence of long tails for large N, which makes it convenient to define the apparent stall force as discussed above. We also notice that for small forces ($F < 10$ pN), the velocity for $N = 10,15,20$ is slightly greater than $V_1(0)$. This effect is a numerical artifact due to the existence of very long transients for large clusters under the action of small forces that bias the statistics to larger velocities. A simple argument shows that this effect cannot be present for purely repulsive potentials. In fact, let us consider a cluster of N motors under an external force F that moves at $V_N(F) > V_1(0)$. The last motor will only be slowed down by the motors in the front since the interaction is repulsive, thus the last motor will have a velocity smaller than $V_1(0)$ and it will fall behind the cluster. By repeating the same reasoning, the cluster will lose all motors except the leading one, which will move at $V_1(0)$, hence $V_1(0) \geqslant V_N(F) \forall N, F > 0$ for the case of a repulsive interaction.

C. Convergence to mean field and the role of diffusion in the staircase shape of VF curves

We have shown that the cooperative action of motor clusters outperforms the simple addition of individual forces, i.e., the extensive scaling $V_N(F) = V_1(F/N)$ or $F_N(V) = NF_1(V)$. This scaling is the one predicted by a mean-field ansatz, which assumes that correlations between positional and internal degrees of freedom of the motors are neglected. In Ref. [23] it was established that the extensive scaling was obtained in the limits of large noise intensity or long-range repulsive interaction between motors. For the case of hard-core repulsion and typical noise intensity values for KIF1A, the latter arguments implied that the mean-field ansatz was essentially correct in the case $\beta = 0$. We have thus shown that $\beta \neq 0$ is responsible for a stronger violation of the mean-field ansatz in the constructive direction, that is, for further enhancement of cooperativity. Here we explicitly show how the introduction of a soft long-range repulsion interaction restores the mean-field scaling. To this aim we add to the hard-core part W_{HC} an exponential repulsive tail of the form

$$W_L(\xi) = \kappa \Lambda e^{-\xi/\Lambda}, \tag{4}$$

where κ measures the strength of the interaction and Λ denotes its range. In Fig. 5 we study the loss of cooperativity for the $N = 5$ curve of Fig. 3 as Λ is increased. We notice that the stall force decreases for increasing Λ and the cooperative mechanism induced by the finite dwell time disappears for sufficiently large Λ, converging to the case $\beta = 0$. Interestingly,

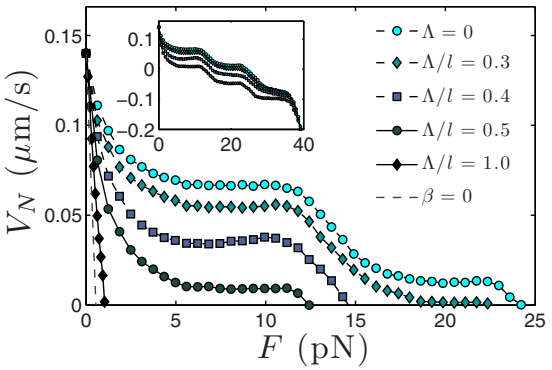

FIG. 5. (Color online) Convergence to mean field in the presence of long-range repulsion with strength $\kappa l/k_BT = 5$ and different Λ. The curve studied corresponds to the case $N = 5$ in Fig. 3. Symbols are calculated for $\beta = 2.5$ and the dashed line corresponds to the case $\beta = 0$. The inset shows VF curves including negative velocities. The staircase behavior persists during backward motion until the recruiting of the totality of motors.

the staircase behavior persists for negative velocities and it is not very sensitive to the long-range interaction for $\Lambda/l < 0.5$ (Fig. 5, inset). Now we study the effect of noise strength on the VF curves. Figure 6 shows the same $N = 5$ curve for four different noise intensities. We notice that oscillations smooth out for low noise intensity. As diffusion is lowered, the external force is able to cluster motors more easily and the recruitment effect is not so pronounced. Hence, sufficiently high diffusivity is required, together with $\beta \neq 0$, to produce staircase-shaped VF curves.

D. Active and passive forces: Cluster force distribution

Each motor in the cluster experiences active and passive forces. Active forces are those forces driven by ATP hydrolysis that allow motors to perform their power stroke. In our context, the power stroke corresponds to the sliding over the ratchet potential when motors decay. Therefore, the average active force for the ith motor reads $F_i^{\rm act} = -\langle U'(x_i,k_i)\rangle$. On the other hand, passive forces correspond to the forces motors experience due to the transmission of the external force F

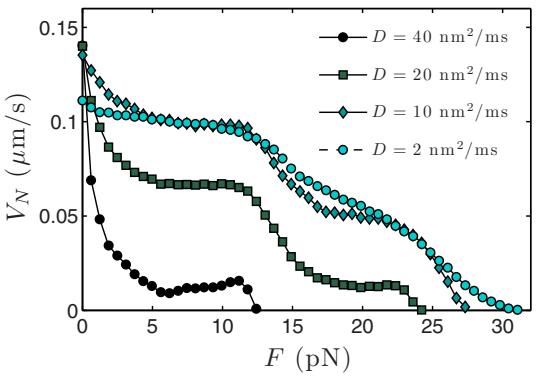

FIG. 6. (Color online) Plot of VF curves for different noise intensities. The curve studied corresponds to the case $N = 5$ in Fig. 3. As diffusion strength is lowered, the staircase behavior smoothes out.

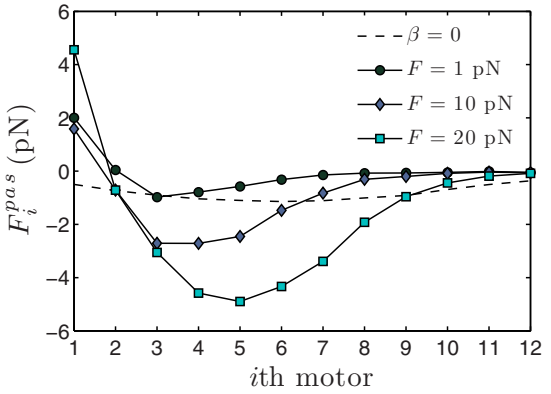

FIG. 7. (Color online) Passive force distribution $F_i^{\rm pas}$ for $N = 12$, $\beta = 1$, and different forces (symbols) and for $\beta = 0$, $F = 10$ pN (dashed line). The force distribution in the cluster shows a pronounced dip, which reflects an enhanced activity of the central part of the cluster in the presence of dwell time.

via the potential W, therefore the average passive force the ith motor experiences reads $F_i^{\rm pas} = -\langle\sum_{k\neq i} W(x_i - x_k)\rangle - F\delta_{1i}$. Hence, computing the time average in (1) we have

$$\lambda\langle\dot{x}_i\rangle = F_i^{\rm act} + F_i^{\rm pas}. \tag{5}$$

Since the average velocity of each motor in the cluster is the same, this last equation tells us that the sum of active and passive forces for each motor is constant on average. In Fig. 7 we measure passive forces $F_i^{\rm pas}$ inside a $N = 12$ cluster for different external forces. By virtue of Eq. (5), the complementary active forces can be obtained by subtraction of the passive ones from the constant term. For $\beta = 0$ the force distribution among motors is fairly homogeneous for our choice of noise intensity and force. However, when $\beta \neq 0$, the force is much more unevenly distributed. Interestingly, the first motor is not active, but is passively pushed by a central group of motors that mostly originate the active forces. This central group of active motors grows as F is increased. The last motors rarely interact with the main cluster and thus they have a minor contribution. The emergence of a nontrivial structure in the internal distribution of forces is a signature of cooperativity in this system and was already noted in Ref. [23] for $\beta = 0$. However, in this case the effect is still present for large noise intensities due to the addition of dwell time.

E. Coordinated motion of large clusters

In the case of large clusters under heavy loads, the cluster adopts a characteristic stepwise coordinated mode, already reported in Ref. [23] for $\beta = 0$. In this configuration, the cluster waits for some collective dwell time before performing a step as a whole, with an almost synchronous stepping of all motors, superposed to the small fluctuations of the individual motors. Steps are totally asymmetric, i.e., no backward stepping occurs. The synchronous displacement is clearer for the leading motors than for the ones in the rear. Figure 8 shows the logarithm of the step size distribution $P(\Delta x)$ measured at each $\Delta t \sim 1$ ms for the leading motor of a $N = 40$ cluster with an external force $F = 30$ pN. The large central peak reflects the small fluctuations of the motor.

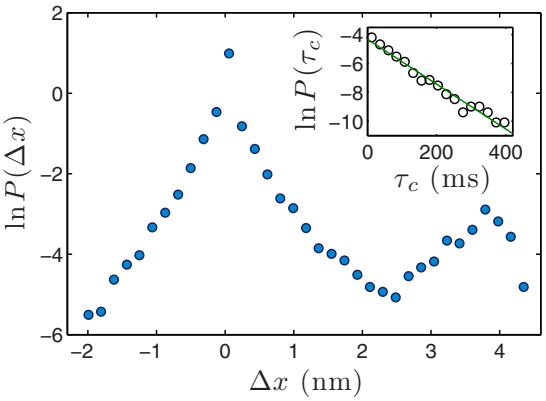

FIG. 8. (Color online) Natural logarithm of the step size distribution $P(\Delta x)$ measured at each time step for the leading motor of an $N = 40$ cluster with a load of $F = 30$ pN. The inset shows the natural logarithm of the collective dwell time distribution $P(\tau_c)$. The green line shows a good fit to an exponential distribution. Measures are taken at each time elapsed between steps $\Delta x \geqslant 2$ nm, which from $P(\Delta x)$ are assumed to contribute to a net movement of the cluster.

The small peak around 4 nm corresponds to the synchronous displacement, which for our choice of σ is roughly half the period of the ratchet. We may identify a collective step as a displacement $\Delta x \geqslant 2$ nm of the first motor so that we can obtain the time distribution $P(\tau_c)$ for the collective dwell time τ_c. This is shown in Fig. 8 (inset). The distribution appears to be very close to exponential and has a mean collective dwell time $\langle \tau_c \rangle \simeq 60$ ms, implying a rather small velocity of $\simeq 70$ nm/s. This mode of transport could be relevant to overcome very large forces in the presence of obstacles or traffic jams, by the recruitment of a sufficient number of motors.

F. Efficiency and randomness

To further characterize the collective properties of motor clusters, we briefly discuss their collective efficiency and randomness. In Fig. 9 we show the collective efficiency defined in Eq. (2) normalized to the maximum value for a single motor. A remarkable increase of the efficiency was already reported for the case $\beta = 0$ in Refs. [22,23], where clusters of ten motors increased the single-motor efficiency by a factor 10. In the presence of dwell time we find that the maximum efficiency for similar clusters may increase up to a factor 100 that of a single motor. As shown in Fig. 9, the efficiency in our case also exhibits complex behavior, as a consequence of the staircase-shaped VF curves. If we take $\Delta\mu \simeq 20 k_B T$ as a reasonable value [25], the maximum efficiency of a single motor is $\eta_1^{\max} \sim 10^{-4}$. The low value is clearly associated with the diffusive part of the motor cycle, which introduces an important number of backward events. In this sense, the presence of other motors contributes to further rectify possible diffusive backward excursions. Notice that the efficiency of a noise-driven motor such as KIF1A is necessarily very small compared to the case of dimeric KIF5, exploiting the hand-over-hand mechanism. Accordingly, the low efficiency of the motor is also associated with a high randomness. This parameter is defined as the ratio of the diffusive versus ballistic displacements of the motor, at the scale of the track periodicity l [26]. We find that the collective randomness decreases very fast with the addition of motors. For the stepwise coordinated mode discussed above, the randomness parameter remains close to 1, that is, the case of a totally biased random walker performing unit steps with an exponentially distributed time.

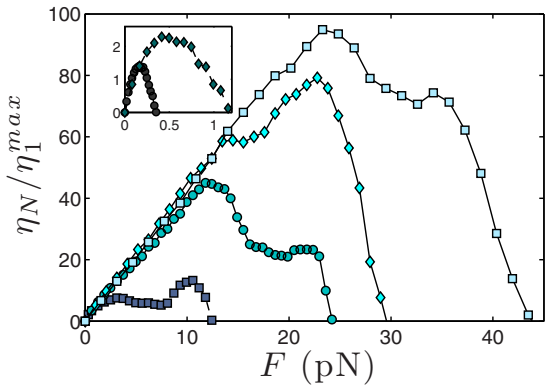

FIG. 9. (Color online) Collective efficiency normalized to the maximum value for $N = 1$. The addition of motors in the cluster greatly enhances the efficiency of the system. The inset shows efficiencies for $N = 2$ and 3. The different parameter values and symbols are the same as in Fig. 3.

IV. CONFINING INTERACTIONS

A. Rigidly coupled motors

Pure hard-core repulsion between motors appears to be a good description to account for excluded volume interactions in the transport of soft cargoes, where motors move freely and motors are unequally loaded. However, the case of rigidly coupled motors separated by a fixed distance is also of important interest in the transport of rigid cargoes and to other situations relevant for biotechnological applications, which can be designed using rigid assemblies of motors [27]. Following Ref. [23] to describe rigid interaction between motors we will use a harmonic potential $W_S(\xi) = \frac{1}{2}k(\xi - d)^2$, where d is the motor-motor distance. We define the dimensionless constant $\bar{k} \equiv k_B T/kl^2$ as a measure of the stiffness of the assembly. Therefore, the limit of rigid coupling will be $\bar{k} \ll 1$. As discussed in Ref. [23], nontrivial dynamic effects can happen when d and l are commensurable. Additionally, for the case $\beta \neq 0$, the strength of the binding interaction can produce a nonmonotonic behavior of the VF curves for a certain force range (Fig. 10, inset). In order to be able to compare our results to the case of nonbounded motors, we typically choose values of $\bar{k}$ and d that minimize such commensurability effects in the rigid limit. In general we observe that velocities at a given force are typically larger than in the hard-core case. This effect is expected since rigid coupling enables not only pushing but also pulling of adjacent motors. The force enhancement due to the presence of dwell time is also found for rigid coupling. In Fig. 10 we show several VF curves for different numbers of motors. Note that for $\beta \neq 0$ the displacement of one motor is strongly conditioned to the motion of the rest. This means that a significant number of motors must be either in the weakly bound state or sliding down the ratchet potential. This

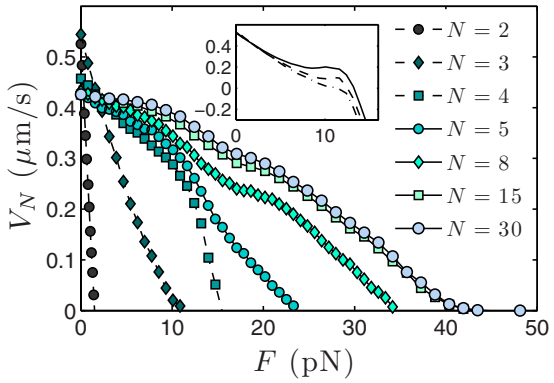

FIG. 10. (Color online) Plot of VF curves for the case of rigid coupling, with $d/l = 1.341$, $\beta = 1.25$, and $\bar{k} = 4 \times 10^{-3}$. The inset shows the $N = 3$ VF curve for $\bar{k} = 10^{-3}, 3 \times 10^{-3}, 4 \times 10^{-3}$ (ordered from more to less bumped).

fact implies an effectively larger dwell time, which in turn implies a faster growth of the stall force with the number of motors. However, the stall force of the system saturates for $N > 15$ at $\simeq$ 35–40 pN (Figs. 10 and 11). On the other hand, we notice that the velocity at null force $V_N(0)$ presents an overshoot for $N = 2,3$ motors and stabilizes for $N \geqslant 5$ (Fig. 11, inset). This effect is due to the fact that the minimum number of consecutive motors over the lower ratchet slope needed to remove a motor from the minima must be greater than $\lfloor l/a - 1 \rfloor$, which in our case is 5 ($a/l = 0.2$). For the case $a = 0$, a given motor in the minima could not be removed by any number of motors and $V_N(0)$ would decay with N until vanishing since the motion of the foremost motor is constrained to the dynamics of the rest.

B. Raft-induced interactions

Lipid rafts are membrane microdomains that float freely in the membrane bilayer. When groups of motors bind specifically to lipid raft domains in vesicles, their motion is constrained by the size of the microdomain [28]. In this section

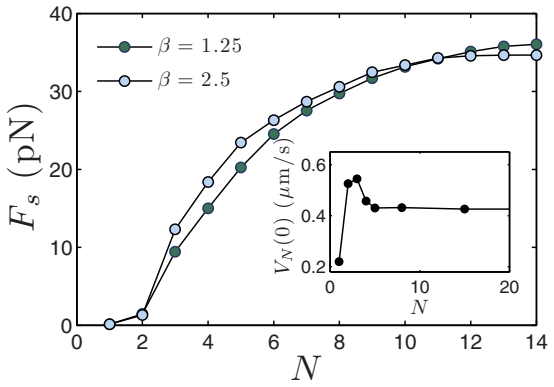

FIG. 11. (Color online) Plot of F_s vs N for $\beta = 1.25, 2.5$; $\bar{k} = 5 \times 10^{-3}$; and $V_c \simeq 10^{-4}$ μm/s. The stall force of the system saturates around 35 pN for $N \simeq 15$ motors. The inset shows $V_N(0)$ vs N using the data in Fig. 10. We appreciate an overshoot on the velocity around $N = 3$ and a rapid stabilization as N increases.

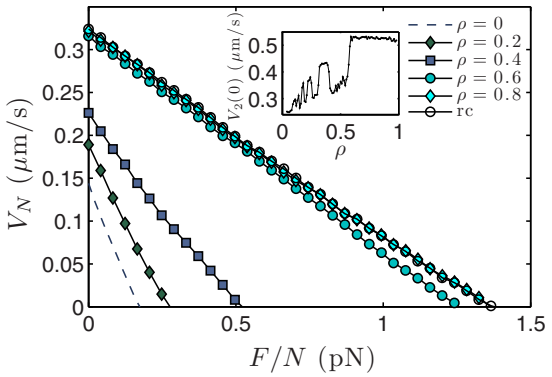

FIG. 12. (Color online) Plot of VF curves for the case of $N = 2$ and raft-induced interactions with $\sigma/l = 0.341$, $\beta = 2.5$, and different raft densities ρ. Open circles denote the VF relationship for the same parameter values and rigid coupling interaction with $\bar{k} = 10^{-3}$. The inset shows the evolution of the velocity of the cluster at null force as a function of ρ for $\beta = 1.25$.

we incorporate such raft-induced confining interactions in our model motivated by the experiments in Ref. [28], where the liposome movement driven by the collective action of Unc104 motors (the analogous kinesin of KIF1A for *C. elegans*) showed a very steep dependence on phosphatidylinositol 4,5-biphosphate concentration due to the formation of lipid rafts. Two different hypotheses were proposed to explain such phenomenon: dimerization of Unc104 motors or cooperativity between the monomeric form of the motors. The aim of this section is to reproduce raftlike conditions and to study the velocity dependence on the parameters describing this effective interaction.

Let us consider a raft of length L that contains N motors of size σ. In order to confine the movement of motors, we will use a truncated Lennard-Jones potential that will depend on the distance between the first and last motor $\phi \equiv x_N - x_1 > 0$. Since motors can only move in a region $L - \sigma$, the potential reads

$$W_R(\xi_r) = 4\epsilon \left[\left(\frac{\sigma}{\xi_r} \right)^{12} - \left(\frac{\sigma}{\xi_r} \right)^{6} \right], \tag{6}$$

where $\xi_r \equiv L - \phi$ and the expression is only valid for $\phi > L - 2^{1/6}\sigma$ and zero otherwise. This potential will be added to the hard-core part only for $i = 1, N$. We define the dimensionless density of the raft as $\rho \equiv N\sigma/L$. In Fig. 12 we study how VF curves change as a function of the raft motor density ρ for $N = 2$, varying L for a fixed motor size σ. The presence of raft-induced interactions confines the motion of the two motors and establishes a well defined mean motor distance as ρ increases. The stall force is greatly enhanced similarly as in the hard-core and rigid coupling cases. Actually, in the limit $\rho \to 1$ the system converges to the rigid coupling case as expected. However, this convergence does not follow a simple monotonic growth but an irregular dependence on ρ (Fig. 12, inset). This dependence is difficult to interpret given the large number of length scales that could lead to commensurability effects with L, namely a, l, σ, and $\langle \xi \rangle$. The velocity of the cluster already converges to the rigid coupling case around $\rho \simeq 0.6$; however, this property is missed for $N = 3$ (data not shown). For $N > 2$, the system shows an intermediate behavior

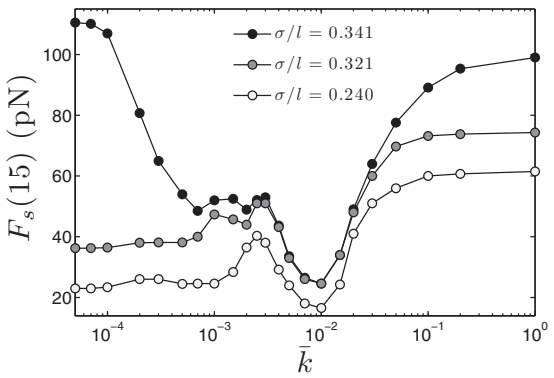

FIG. 13. Stall force for $N = 15$ vs $\bar{k}$ showing the transition between rigid coupling and hard-core interaction for different motor sizes σ and $\beta = 1.25$. A pronounced dip appears for a certain $\bar{k}$ range in which the stall force is considerably reduced.

between hard-core repulsion and strong coupling. Consequently, raftlike interactions can speed up the system eliciting velocities of $\sim$0.3–0.5 μm/s, but these are still far from typical liposome velocities ($\sim$1 μm/s) of Unc104 [28]. This suggests that the switching behavior of the liposome movement found in Ref. [28] is probably due to dimerization of Unc104 motors.

C. Transition between rigid coupling and hard-core repulsion

We have previously seen that both rigid and hard-core interactions produce a nonlinear enhancement on the stall force of the system. In this section we explore the transition between these two regimes by changing the parameter $\bar{k}$ in the limit of large N. In order for the transition to be smooth, we use $W_{HC-S}(\xi) = W_{HC}(\xi) + W_S(\xi)$ by setting a motor-motor distance d and a motor size σ. In Fig. 13 we study the dependence of $F_s(15)$ on $\bar{k}$ for three values of the motor size σ. The strength of motor fluctuations $\langle(\xi - d)^2\rangle$ determines the appearance of commensurability effects. Two main factors change the strength of these fluctuations: the rigidity of the interaction $\bar{k}$ and the external load F. For very strong spring constants motors barely fluctuate and commensurability effects are predominant, thus the system is very sensitive to σ and we find strong resonances on the stall force. On the other hand, as we approach the hard-core limit, fluctuations are still small since we are found near stall conditions. In this case, the system resembles the rigid case except for some long excursions of the motors in the rear of the cluster. Thus, motor size effects are present in both the rigid and hard-core limits near stall conditions; however, in the hard-core limit resonances are less pronounced. We notice the presence of a pronounced dip around $\bar{k} \simeq 10^{-2}$. Hence, a weak binding interaction between motors leads to a decrease of the collective stall force in the large-N limit. This can be explained in simple terms. Let us consider a large cluster of weakly bound motors in stall conditions such that the cluster is compressed in the front and only the last motors can fluctuate significantly. Suppose that a fluctuation drives the last motor one step backward and the binding interaction is sufficiently strong that the cluster experiences a restoring force that adds to the external force. Consequently, fluctuations in the rear of the cluster will tend to destabilize it. For this situation to occur, the energy of the interaction must be comparable to the energy scale of the ratchet for $\xi \sim l$, that is, $\bar{k}_c \sim k_B T/U \sim 10^{-2}$. However, if motors do not experience any binding interaction, fluctuations do not affect the cluster.

V. DISCUSSION AND CONCLUSION

We have proposed a two-state noise-driven mechanism to study the collective action of single-headed KIF1A motors *in vitro* extending the study in Ref. [24], which in turn extended the previous work for the case of vanishing dwell time [22,23]. The presence of finite dwell time in the system reveals nontrivial phenomena associated with a great enhancement on the collective force generation of motors and to staircase-shaped velocity-force curves that arise in the high diffusion limit. The cooperative mechanism of force generation seems to be robust within a variety of motor-motor interactions. This effect is able to produce a two-order-of-magnitude gain on the collective efficiency up to values of $\sim 10^{-2}$ (typical efficiencies for individual noise-driven motors may be of the order of $\sim 10^{-4}$ [25]). The range of maximal forces KIF1A motors can achieve depends considerably on the choice of the ratchet height U and the ratio between the average decay and excitation rates β in our model. A reasonable predicted range would be around 20–60 pN for clusters of approximately ten motors, implying that KIF1A would be able to outperform KIF5 collectively in cooperative tasks, despite its poor individual performance. In simple terms, the combination of several motors in a two-state ratchet enables a switch from a low-force noise-driven mechanism ($\sim k_B T l/l_D^2$) to a filament-binding mechanism with a high-force scale ($\sim U/l$). The collective stall force at a given velocity grows faster than proportional to N up to around five KIF1A motors. This behavior is remarkably different for KIF5, whose collective forces are weakly dependent on the number of motors in this regime [12,29]. For $N \sim$ 5–10 the force scaling of KIF1A remains roughly proportional to the number of motors, a property that is missed by KIF5 according to lattice models [10]. Finally, for large N the total force produced by the motor ensemble eventually saturates to values that can eventually surpass those achieved collectively by KIF5.

The presence of dwell time typically produces an increase on the velocity at a given force per motor, especially in the case of rigid coupling or raft-induced interactions where diffusion is effectively reduced within the cluster. However, the maximum twofold increase of the velocity seems insufficient to explain some reported *in vivo* velocities of Unc104 ($\sim$1 μm/s) [28]. With regard to this point, it is worth recalling that dimerization of KIF1A has been reported *in vivo*, preserving the alternation between a weakly bound diffusive state and a strongly bound state. Under these circumstances, the coexistence of possible hand-over-hand stepping and a diffusive state could result in a similar mechanism of cooperativity, while the overall velocity could be significantly increased.

In this article we have provided a thorough numerical study of the collective action of single-headed KIF1A motors based on Brownian dynamics. We predict a dramatic improvement of the collective performance of these motors for tasks associated with the transport of membrane-bound cargoes. The results

rely on a two-state noise-driven model that successfully explains the motion of a single motor. While the extension to interacting motors seems plausible, it remains unclear to what extent this modeling is sufficiently realistic for large numbers of motors. A salient feature of our results for relatively small motor clusters is that the collective VF curves have staircase shapes, which effectively count the number of active motors in the cluster. This could potentially be used to infer information about forces in situations where resolving individual motors may be more feasible than measuring forces directly. From a biological point of view, our results reinforce the hypothesis that the specificity of KIF1A to axonal vesicular trafficking is due to its unique adaptation to cooperative force generation. From a fundamental physics point of view, we have shown that Brownian motors based on two-state ratchets with independent switching and under unequal loading are remarkably adapted to cooperative force generation. Within this spirit, rectification mechanisms and spatial confinement in ratchet systems may be deeply related to the emergence of cooperativity in nanoscopic transport [30]. Additionally, hydrodynamic coupling in thermal ratchet motion might also play an important role [31].

Finally, analytical results might be possible using a discrete approach. Lattice models for KIF1A have already been shown to be suitable to study shock formation and nonequilibrium phase transitions [16,32,33]. In order to incorporate cooperative effects in such models, transitions of blocks of adjacent motors should be incorporated similarly to what was proposed in Ref. [24]. This effect is especially relevant in the case of large clusters under heavy loads as discussed in Sec. III E. On the other hand, recent evidence shows that lattice models might be suitable to describe confinement situations. Systems investigated recently include coupled molecular motors [34] and coupled molecular spiders [35].

ACKNOWLEDGMENTS

We acknowledge financial support under Projects No. FIS2010-21924-C02-02 and No. 2009-SGR-014. D.O. also acknowledges a FPU grant from the Spanish Government.

[1] B. Alberts, A. Johnson, J. Lewis, M. Raff, K. Roberts, and P. Walter, *Molecular Biology of the Cell*, 4th ed. (Garland, New York, 1994).
[2] J. Howard, *Mechanics of Motor Proteins and the Cytoskeleton* (Sinauer, Sunderland, MA, 2001).
[3] N. Hirokawa, Y. Noda, Y. Tanaka, and S. Niwa, Nat. Rev. Mol. Cell Biol. **10**, 682 (2009).
[4] E. L. F. Holzbaur and Y. E. Goldman, Curr. Opin. Cell Biol. **22**, 4 (2010).
[5] N. Hirokawa and R. Takemura, Nat. Rev. Mol. Neurosci. **6**, 201 (2005).
[6] N. Hirokawa, S. Niwa, and Y. Tanaka, Neuron **68**, 610 (2010).
[7] C. Kaether, P. Skehel, and C. G. Dotti, Mol. Biol. Cell **11**, 1213 (2000).
[8] G. B. Stokin, C. Lillo, T. L. Falzone, R. G. Brusch, E. Rockenstein, S. L. Mount, R. Raman, P. Davies, E. Masliah, D. S. Williams, and L. S. Goldstein, Science **307**, 1282 (2005).
[9] S. Millecamps and J.-P. Julien, Nat. Rev. Neurosci. **14**, 161 (2013).
[10] O. Campàs, Y. Kafri, K. B. Zeldovich, J. Casademunt, and J. F. Joanny, Phys. Rev. Lett. **97**, 038101 (2006).
[11] O. Campàs, C. Leduc, P. Bassereau, J. Casademunt, J. F. Joanny, and J. Prost, Biophy. J. **94**, 5009 (2008).
[12] A. K. Rai, A. Rai, A. J. Ramaiya, R. Jha, and R. Mallik, Cell **152**, 172 (2013).
[13] Y. Okada and N. Hirokawa, Science **283**, 1152 (1999).
[14] Y. Okada and N. Hirokawa, Proc. Natl. Acad. Sci. USA **97**, 640 (2000).
[15] Y. Okada, H. Higuchi, and N. Hirokawa, Nature (London) **424**, 574 (2003).
[16] K. Nishinari, Y. Okada, A. Schadschneider, and D. Chowdhury, Phys. Rev. Lett. **95**, 118101 (2005).
[17] M. Kondo, Y. Takei, and N. Hirokawa, Neuron **73**, 743 (2012).
[18] F. Jülicher, A. Adjari, and J. Prost, Rev. Mod. Phys. **69**, 1269 (1997).
[19] P. Reimann, Phys. Rep. **361**, 57 (2002).
[20] D. Chowdhury, Phys. Rep. **529**, 1 (2013).
[21] J. W. Hammond, D. Cai, T. L. Blasius, Z. Li, Y. Jiang, G. T. Jih, E. Meyhofer, and K. J. Verhey, PLoS Biol. **7**, e1000072 (2009).
[22] J. Brugués and J. Casademunt, Phys. Rev. Lett. **102**, 118104 (2009).
[23] J. G. Orlandi, C. Blanch-Mercader, J. Brugués, and J. Casademunt, Phys. Rev. E **82**, 061903 (2010).
[24] D. Oriola and J. Casademunt, Phys. Rev. Lett. **111**, 048103 (2013).
[25] A. Parmeggiani, F. Jülicher, A. Ajdari, and J. Prost, Phys. Rev. E **60**, 2127 (1999).
[26] A. B. Kolomeisky and M. E. Fisher, Annu. Rev. Phys. Chem. **58**, 675 (2007).
[27] T. Korten, A. Månsson, and S. Diez, Curr. Opin. Biotechnol. **21**, 477 (2010).
[28] D. R. Klopfenstein, M. Tomishige, N. Stuurmand, and R. D. Vale, Cell **109**, 347 (2002).
[29] K. Furuta, A. Furuta, Y. Y. Toyoshima, M. Amino, K. Oiwa, and H. Kojima, Proc. Natl. Acad. Sci. USA **110**, 501 (2013).
[30] P. Malgaretti, I. Pagonabarraga, and J. Miguel Rubi, J. Chem. Phys. **138**, 194906 (2013).
[31] P. Malgaretti, I. Pagonabarraga, and D. Frenkel, Phys. Rev. Lett. **109**, 168101 (2012).
[32] P. Greulich, A. Garai, K. Nishinari, A. Schadschneider, and D. Chowdhury, Phys. Rev. E **75**, 041905 (2007).
[33] J. Sparacino, P. W. Lamberti, and C. M. Arizmendi, Phys. Rev. E **84**, 041907 (2011).
[34] C. Keller, F. Berger, S. Liepelt, and R. Lipowsky, J. Stat. Phys. **150**, 205 (2013).
[35] M. Rank, L. Reese, and E. Frey, Phys. Rev. E **87**, 032706 (2013).